Supporting Information

Increased crystallinity of RuSe₂/carbon nanotubes for enhanced electrochemical hydrogen generation performance

Dongze Li [a,b], Meng Zha [b,c], Ligang Feng[b,*], Guangzhi Hu[a,c], Chaoquan Hu[d*], Xiang Wu[e] and Xinzhong Wang [a*]

[a] Information Technology Research Institute, Shenzhen Institute of Information Technology, Shenzhen, 518172, China; wangxz@sziit.com.cn

[b] School of Chemistry and Chemical Engineering, Yangzhou University, Yangzhou 225002, China. Email: ligang.feng@yzu.edu.cn; fenglg11@gamil.com

[c] State Key Laboratory of Multiphase Complex Systems, Institute of Process Engineering, Chinese Academy of Sciences, Beijing 100190, P. R. China. E-mail: cqhu@ipe.ac.cn

[d] Institute for Ecological Research and Pollution Control of Plateau Lakes, School of Ecology and Environmental Science, Kunming 650504, China. State Key Laboratory of Multiphase Complex

[e] School of Materials Science and Engineering, Shenyang University of Technology, Shenyang 110870, Liaoning, China

Experimental section

Materials and Chemicals

All chemicals used in the experiment were of analytic grade purity and were used as received without further purification. Ethylene glycol ($C_2H_6O_2$), selenium dioxide (SeO_2), Ruthenium chloride hydrate ($RuCl_3 \cdot xH_2O$) and Ruthenium were purchased from Shanghai Aladdin Bio-Chem Technology Co., Ltd. Potassium hydroxide (KOH) was bought from the Sinopharm Chemical Reagent Co., Ltd. Commercial Pt/C catalyst was purchased from Johnson Matthey Chemicals Ltd for reference. The ultrapure water was used in all experiments (18.2 MΩ) (Thermo Fisher Scientific (USA) Co., Ltd).

Synthesis of fresh RuSe$_2$/CNTs

The fresh $RuSe_2$ catalyst was prepared via a microwave irradiation-assisted-reduction approach. Firstly, 50 mg SeO_2 and 100 mg carbon nanotube were dispersed with 50 mL ethylene glycol in a bunsen flask, and then 2 mL $RuCl_3$ aqueous solution (Ru: 19.4 mg/mL) was added into the mixture. After stirring for 30 min until forming the well-dispersed suspension, the proper amount of 0.1M KOH solution was added into the flask aiming to adjust the pH to neutral. Secondly, the suspension was irradiated by the solid-liquid microwave synthesizer at 800 W for 3 min. The catalyst powder was obtained through filtration, purification by ultrapure water, and dried in a vacuum oven at 60 °C for 10 hours, and the obtained catalyst was named fresh RuSe$_2$/CNTs.

Synthesis of crystallized RuSe$_2$/CNTs-T

The $RuSe_2$ product was transferred to a quartz tube with a thermal annealing temperature at 650 °C under the N_2 atmosphere for 2 h. The as-obtained samples were denoted as RuSe$_2$/CNTs-650; The $RuSe_2$ thermal annealed at 550 °C and 750 °C in the same condition was also done and the finally obtained catalysts were denoted as RuSe$_2$/CNTs-550, and RuSe$_2$/CNTs-750 respectively.

Synthesis of Ru/CNTs

The Ru/CNTs catalyst as the control sample was prepared following the same procedure without adding SeO_2.

Physical Characterization

The X-ray diffraction characterizations were carried out on the Bruker D8 advance X-ray diffraction (XRD) with Cu Kα radiation. The sample morphologies were examined with an FEI Sirion-200 scanning electron microscope (SEM) and a transmission electron microscope (TEM) operating at 200 kV. Energy-dispersive X-ray spectroscopy (EDS) images are obtained on a FEI-Talos F200X transmission electron microscope (acceleration voltage: 200 kV). And the X-ray photoelectron spectroscopy (XPS) measurement is carried on the Thermofisher Escalab 250 Xi$^+$ system.

Electrochemical measurement

All the chemical measurements were performed with a Bio-Logic VSP electrochemical workstation (Bio-Logic Co., France) and a conventional three-electrode system. The glassy carbon electrode (3 mm diameter, 0.07 cm^2) was used as the working electrode; a saturated calomel electrode (SCE) was served as the reference electrode in the acid elelctrlyte and a mercury/mercury oxide electrode (Hg/HgO) was used as the reference electrode in the alkaline electrolyte; a graphite rod was chosen as the counter electrode. All potentials were converted and referred to the reversible hydrogen electrode unless otherwise noted. The preparation method of the working electrodes containing investigated catalysts is as follows. In short, 2 mg of catalyst powder was uniformly dispersed in the mixed solution of 950 μL absolute ethyl alcohol and 50 μL Nafion solution (5wt.%, Sigma-Aldrich), then the mixture was ultrasonicated for 20 min to generate a homogeneous ink.

Next, 5 μL of catalyst ink was dropped on the surface of the glassy carbon electrode and dried at room temperature. The bare glassy carbon electrode was always polished and cleaned with alumina slurry (0.05 μm) before the test.

For HER measurement, the linear sweep voltammograms (LSV) and cyclic voltammograms (CV) of all catalysts were recorded at a scan rate of 5 mV s^{-1} in the acid and alkaline electrolyte and all the HER polarization curves are presented without iR-correction for further analysis. For the IR-correct polarization curve, 85% of the uncompensated resistance obtained from EIS plots was used for IR-correction (ca. 7~9 Ω).

Tafel slope analysis

The overpotential values were defined by the Tafel equation: η=a+blog|j|, where η was the applied overpotential, j was the current density, the Tafel slope (b) can be obtained.

ECSA measurements and calculation

The electrochemical active surface area can be calculated from the equation ECSA=R_f*S, where S was generally equal to the geometric area of the electrode (in this work, S=0.07 cm^2). The R_f was determined by the relation R_f=C_{dl}/(40*0.07) on basis of the double-layer capacitance (C_{dl}) of a smooth metal surface (40 μF cm^{-2}).[1, 2]

Specific activity and Turnover frequency

The specific activity was obtained by normalizing the apparent current to ECSA. The TOF (s^{-1}) for HER can be calculated with the following equation TOF (s^{-1}) = I/(2*F*n), where I is the current (A) during linear sweep measurement, F is the Faraday's constant (96485.3 C/mol), n is the number of active sites (mol). The factor 1/2 is based on the consideration that two electrons are required to produce one hydrogen molecule.[2, 3]

Electrochemical Impedance Spectroscopy analysis

The electrochemical impedance spectra (EIS) were recorded at the frequency range from 1000 kHz to 10 mHz. The amplitude of the sinusoidal potential signal was 5 mV.

Stability test and chronoamperometry measurements

The dynamical stability was tested for 1000 cycles at the constant scan rate of 50 mV s^{-1}. After 1000 cycles, the polarization curve was recorded for comparison with the initial curve. To estimate the stability of the catalysts, chronoamperometry (CA) was performed at a fixed potential for a long-term measurement.

Faraday efficiency

The working electrode was prepared by drop-casting catalyst suspension on the glassy carbon electrode with a surface area of 0.07 cm^{-2}. A constant potential for HER was applied on the electrode and evolved gas was continually recorded, respectively. Thus, the faradaic yield was calculated from the ratio of V$_{experimental}$ (the recorded gas volume) to V$_{theoretical}$ (the theoretical gas volume) during the charge transport process.

The Faradic efficiency of HER was calculated with the following equation:

$$Faradaic\ yield = \frac{V_{experimental}}{V_{theoretical}} = \frac{V_{experimental}}{\frac{1}{2} \times \frac{Q}{F} \times V_m}$$

where Q is the charge passed through the electrode, F is Faraday constant (96485 C mol^{-1}), the number 2 means 2 molar electrons per mole H$_2$, the number 1 means 1 mole H$_2$, V$_m$ is the molar volume of gas (24.5 L mol^{-1}, 298 K, 101 KPa).
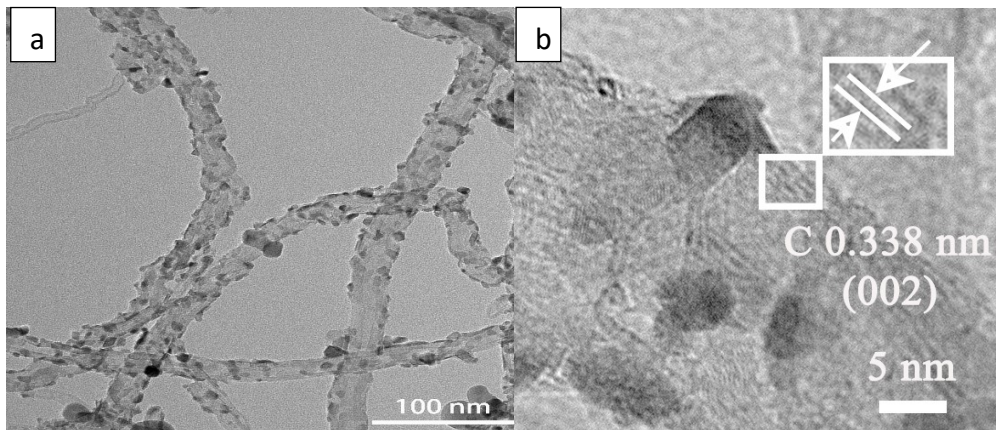
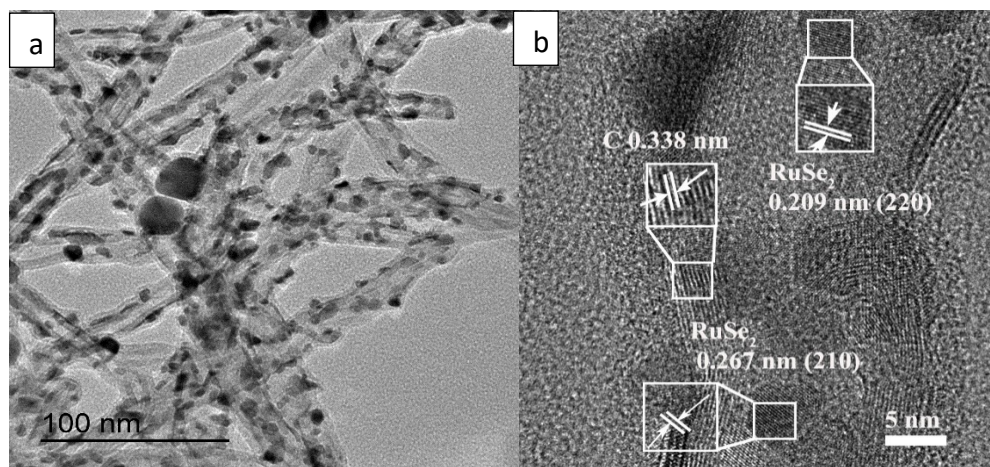**Figure S1.** The TEM images of freshly prepared RuSe$_2$/CNTs.

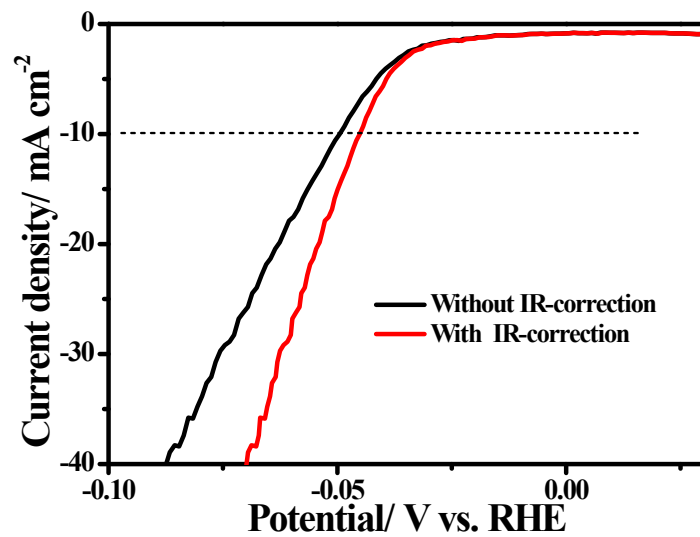**Figure S2.** The TEM image (a) and HRTEM image (b) of RuSe$_2$/CNTs-650.

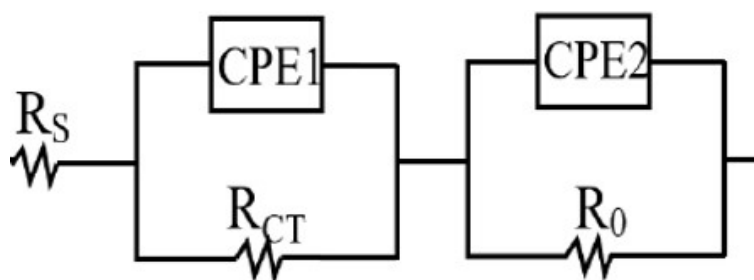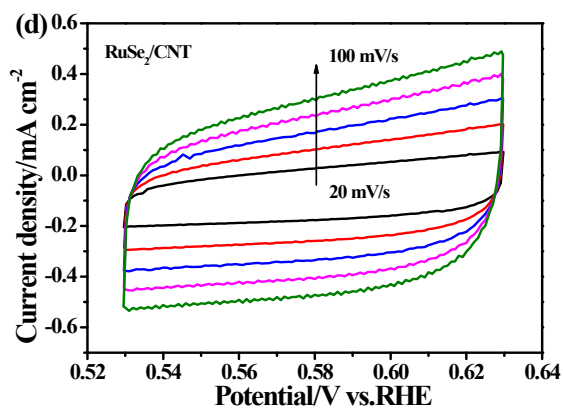**Figure S3.** The polarization curves of RuSe$_2$/CNTs-650 with and without IR-correction in 1 M KOH solution at 5 mV s^{-1}.

**Figure S4.** Equivalent circuit diagram used to fit the Nyquist plots.

In the equivalent circuit, where R_s was the resistance of the electrolyte and the intrinsic resistance of the active materials that were modified on the electrode, R_{ct} represented the charge transfer resistance and R_0 for the adsorption resistance. CPE1 and CPE2 represented the capacitance components for the fitting.
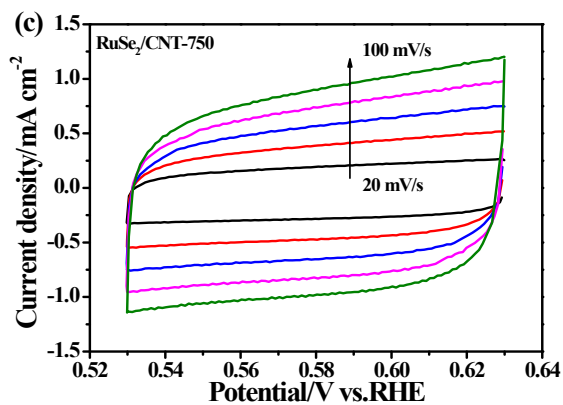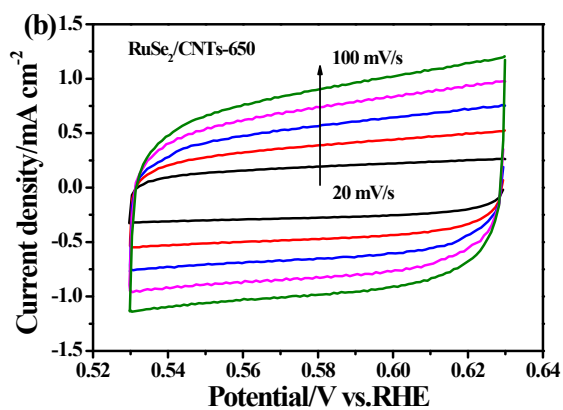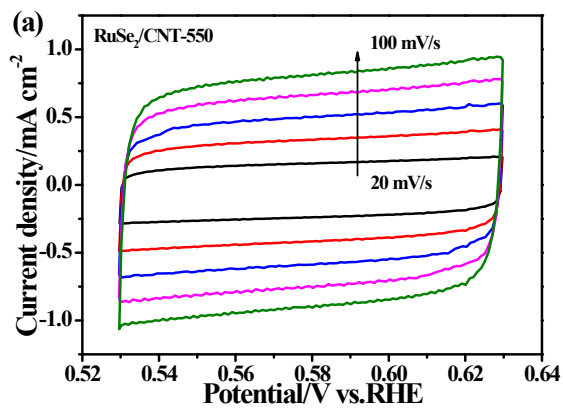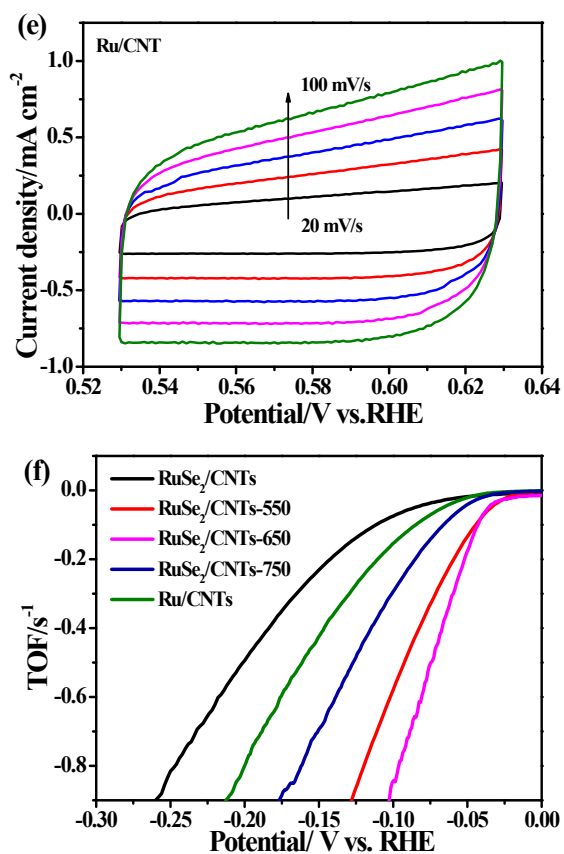
Figure S5. Cyclic voltammograms for the double layer capacitance from 0.53 V to 0.63 V of catalysts RuSe$_2$/CNTs-550 (a), RuSe$_2$/CNTs-650 (b), RuSe$_2$/CNTs-750 (c), RuSe$_2$/CNTs (d), and Ru/CNTs (e) and the TOF curves (f) of RuSe$_2$/CNTs-650 and reference catalysts in 1 M KOH solution.
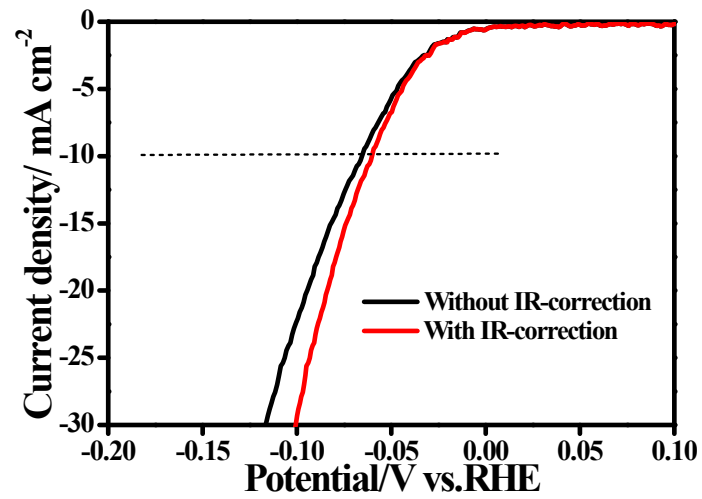
Figure S6. The polarization curves of RuSe$_2$/CNTs-650 with and without IR-correction in 0.5 M H$_2$SO$_4$ solution at 5 mV s^{-1}.
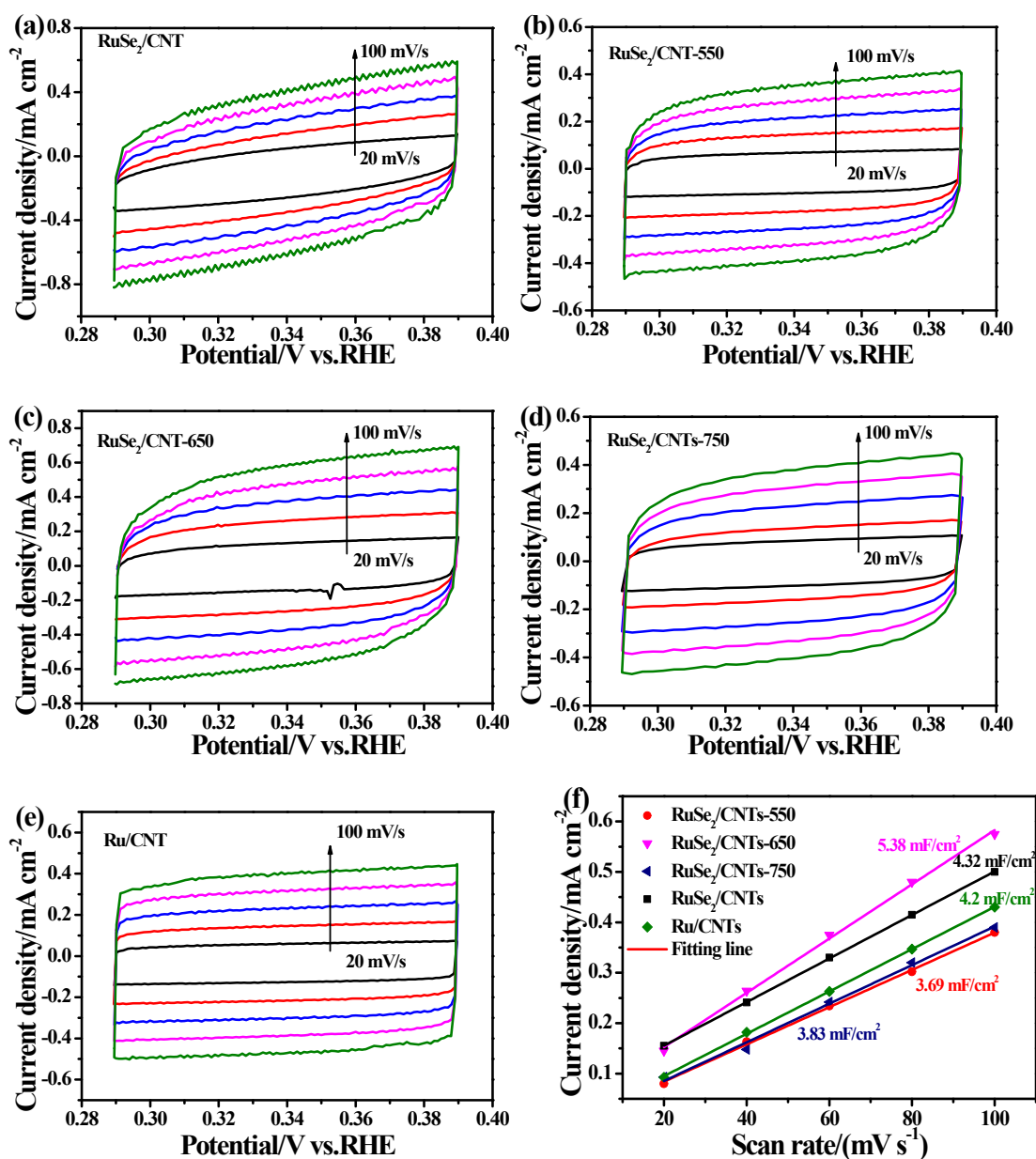
Figure S7. Cyclic voltammograms for the double layer capacitance from 0.29 V to 0.39 V of catalysts RuSe$_2$/CNTs (a), RuSe$_2$/CNTs-550 (b), RuSe$_2$/CNTs-650 (c), RuSe$_2$/CNTs-750 (d), and Ru/CNTs (e) and the linear plots (f) of the capacitive current density versus the scan rates in 0.5 M H$_2$SO$_4$ solution.
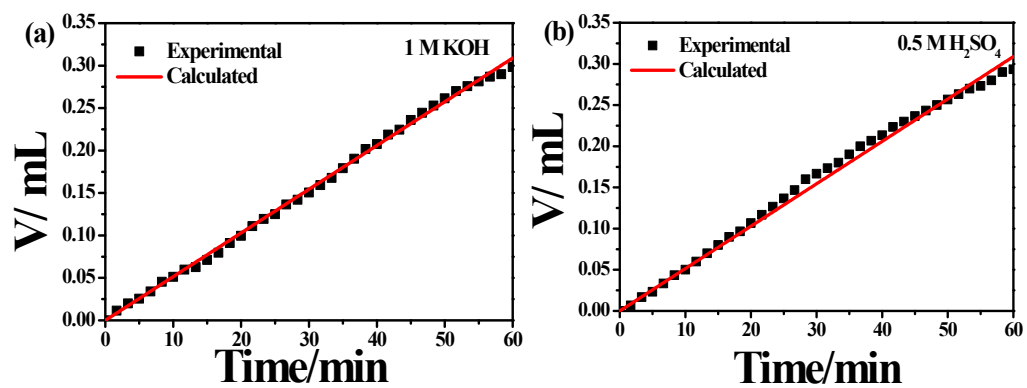
Figure S8. Theoretically calculated and experimentally measured H$_2$ amount versus time for RuSe$_2$/CNTs-650 in (a) 1.0 M KOH and (b) 0.5 M H$_2$SO$_4$ solution, respectively.

Table S1. The high-resolution XPS analysis of Ru 3p for RuSe$_2$/CNTs-650 and RuSe$_2$/CNTs.

catalysts	Ru 3p$_{3/2}$		Ru 3p$_{1/2}$		Content/%
	Peak	Binding energy/eV	peak	Binding energy/eV	
RuSe$_2$/CNTs-650	Ru^0	462.0	Ru^0	484.1	65.9
	Ru^{4+}	463.8	Ru^{4+}	485.9	34.1
RuSe$_2$/CNTs	Ru^0	461.6	Ru^0	483.7	64.0
	Ru^{4+}	463.4	Ru^{4+}	485.5	36.0

Table S2. The high-resolution XPS analysis of Se 3d for RuSe$_2$/CNTs-650 and RuSe$_2$/CNTs.

Catalysts	3d$_{5/2}$		3d$_{3/2}$		Se-O	
	Binding energy/eV	Content/%	Binding energy/eV	Content/%	Binding energy/eV	Content/%
RuSe$_2$/CNTs-650	54.7	49.7	55.6	36.5	58.4	13.8
RuSe$_2$/CNTs	55.0	39.1	55.9	28.8	58.7	32.1

Table S3. Comparison of some representative HER electrocatalysts in alkaline solution.

Catalysts	Solution	Overpotential/mV	Reference
Ru/CoO	1 M KOH	55	[4]
Ru@CQDs	1 M KOH	65	[5]
(MIL-53(Ru-NiFe)@NF	1 M KOH	62	[6]
Ru/C-H_2O/CH_3CH_2OH	1 M KOH	53	[7]
Ru/BP2000	1 M KOH	54.2	[8]
CF@Ru-CoCH NWs	1 M KOH	66	[9]
Ru doped Ni(OH)(2)/TM-0.2	1 M KOH	135	[10]
Ru-NPC	1 M KOH	78	[11]
Ru@RuO_2	0.1 M KOH	137	[12]
SA-Ru-MoS_2	1 M KOH	76	[13]
Co-Ru-MoS_2	1 M KOH	52	[14]
$RuSe_2$/CNTs-650	1 M KOH	48	This work

Table S4. The detailed EIS fitting parameters from equivalent circuits for different catalysts in alkaline solution.

catalysts	R_S/Ω	CPE1/S	R_{CT}/Ω	CPE2/S	R_0/Ω
RuSe$_2$/CNTs-550	8.579	2.828E-4	432.5	1.253E-3	25.2
RuSe$_2$/CNTs-650	7.37	6.732E-4	66.8	3.608E-3	26.5
RuSe$_2$/CNTs-750	7.138	3.061E-4	594.5	1.366E-3	15.3
RuSe$_2$/CNTs	8.576	1.206E-3	5644	1.573E-2	12.55
Ru/CNTs	8.82	1.217E-3	3212	1.435E-3	15.4

Table S5. Double-layer capacitance (C_{dl}) and electrochemical active surface areas (ECSA) of the RuSe$_2$/CNTs-550, RuSe$_2$/CNTs-650, RuSe$_2$/CNTs-750, RuSe$_2$/CNTs, and Ru/CNTs in 1 M KOH solution.

Catalysts	C_{dl} （mF/cm^{-2}）	ECSA （cm^2）
RuSe$_2$/CNTs-550	8.45	14.79
RuSe$_2$/CNTs-650	8.75	15.31
RuSe$_2$/CNTs-750	8.4	14.7
RuSe$_2$/CNTs	3.88	6.79
Ru/CNTs	6.79	11.88

Table S6. The specific activity of the RuSe$_2$/CNTs-550, RuSe$_2$/CNTs-650, RuSe$_2$/CNTs-750, RuSe$_2$/CNTs, and Ru/CNTs at the potential of -0.075 V vs. RHE and TOFs at the potential of -0.075 V vs. RHE in 1 M KOH solution.

Catalysts	Specific activity/mA cm^{-2}	TOF/s^{-1}
RuSe$_2$/CNTs-550	0.108	0.32
RuSe$_2$/CNTs-650	0.136	0.51
RuSe$_2$/CNTs-750	0.052	0.14
RuSe$_2$/CNTs	0.032	0.033
Ru/CNTs	0.031	0.071

Table S7. Comparison of some representative HER electrocatalysts in acidic solution.

Catalysts	Solution	Overpotential/mV	Reference
Te@Ru	0.5 M H_2SO_4	86	[15]
Ru@Co/N-CNTs	0.5 M H_2SO_4	92	[16]
Ru-MoS$_2$/CL	0.5 M H_2SO_4	100	[17]
Ru-W	0.5 M H_2SO_4	85	[18]
Ru-NPC	0.5 M H_2SO_4	93	[11]
Ru-SA/Ti$_3$C$_2$T$_x$	0.1 M $HClO_4$	70	[19]
Ru-CeO$_2$	0.5 M H_2SO_4	74	[20]
C$_3$N$_4$-Ru-F	0.5 M H_2SO_4	140	[21]
RuO$_2$/Co$_3$O$_4$–RuCo@NC-1.95	0.5 M H_2SO_4	141	[22]
RuSe$_2$/CNTs-650	0.5 M H_2SO_4	60	This work

Table S8. The detailed EIS fitting parameters from equivalent circuits for different catalysts in acid solution.

Catalysts	R_S	CPE1	R_{CT}	CPE2	R_0
RuSe$_2$/CNTs-550	9.04	2.21E-4	166.3	1.484E-3	4.05
RuSe$_2$/CNTs-650	8.91	8.188E-3	150	1.305E-3	9.0
RuSe$_2$/CNTs-750	8.10	4.966E-4	278.6	9.333E-5	2.29
RuSe$_2$/CNTs	7.78	5.199E-4	507.2	4.613E-2	38.8
Ru/CNTs	7.56	5.133E-4	366.7	2.036E-2	68.6

Table S9. Double-layer capacitance (C_{dl}) and electrochemical active surface areas (ECSA) of the RuSe$_2$/CNTs-550, RuSe$_2$/CNTs-650, RuSe$_2$/CNTs-750, RuSe$_2$/CNTs, and Ru/CNTs in 0.5 M H$_2$SO$_4$ solution.

Catalysts	C_{dl}（mF/cm^{-2}）	ECSA（cm^2）
RuSe$_2$/CNTs-550	3.69	6.46
RuSe$_2$/CNTs-650	5.38	9.42
RuSe$_2$/CNTs-750	3.83	6.7
RuSe$_2$/CNTs	4.32	7.56
Ru/CNTs	4.2	7.35

Table S10. The specific activity of the $RuSe_2$/CNTs-550, $RuSe_2$/CNTs-650, $RuSe_2$/CNTs-750, $RuSe_2$/CNTs, and Ru/CNTs at the potential of -0.1 V vs. RHE and TOFs at the potential of -0.1 V (vs. RHE) in 0.5 M H_2SO_4 solution.

Catalysts	Specific activity/mA cm^{-2}	TOF/s^{-1}
$RuSe_2$/CNTs-550	0.139	0.19
$RuSe_2$/CNTs-650	0.166	0.38
$RuSe_2$/CNTs-750	0.131	0.16
$RuSe_2$/CNTs	0.046	0.08
Ru/CNTs	0.104	0.14

Reference:

1. L. Zhang, X. Ren, X. Guo, Z. Liu, A. M. Asiri, B. Li, L. Chen and X. Sun, *Inorg. Chem.*, 2018, **57**, 548-552.

2. F. Jinxian, W. Jinqi, T. Yexiang and G.-R. Li, *J Am Chem Soc*, 2018, **140**, 610-617.

3. Z.-Z. Liu, X. Shang, B. Dong and Y.-M. Chai, *Journal of Catalysis*, 2018, **361**, 204-213.

4. J.-X. Guo, D.-Y. Yan, K.-W. Qiu, C. Mu, D. Jiao, J. Mao, H. Wang and T. Ling, *Journal of Energy Chemistry*, 2019, **37**, 143-147.

5. W. Li, Z. Wei, B. Wang, Y. Liu, H. Song, Z. Tang, B. Yang and S. Lu, *Materials Chemistry Frontiers*, 2020, **4**, 277-284.

6. M. Zhao, H. Li, W. Li, J. Li, L. Yi, W. Hu and C. M. Li, *Chemistry – A European Journal*, 2020, **26**, 17091-17096.

7. Y. Li, J. Abbott, Y. Sun, J. Sun, Y. Du, X. Han, G. Wu and P. Xu, *Appl. Catal., B*, 2019, **258**, 117952.

8. H. Hu, F. M. D. Kazim, Q. Zhang, K. G. Qu, Z. H. Yang and W. W. Cai, *ChemCatChem*, 2019, **11**, 4327-4333.

9. J. Li, Q. Zhou, Z. Shen, S. Li, J. Pu, C. Zhong, M. Cao, X. Jin, H. Zhang, Y. Wang and H. Ma, *Electrochim. Acta*, 2020, **331**, 135367.

10. Y. J. Wang, J. K. Wang, T. P. Xie, Q. Y. Zhu, D. Zeng, R. Li, X. D. Zhang and S. L. Liu, *Appl. Surf. Sci.*, 2019, **485**, 506-512.

11. C. Wu, S. Ding, D. Liu, D. Li, S. Chen, H. Wang, Z. Qi, B. Ge and L. Song, *Research*, 2020, **2020**, 5860712.

12. R. Jiang, D. T. Tran, J. Li and D. Chu, *Energy & Environmental Materials*, 2019, **2**, 201-208.

13. J. M. Zhang, X. P. Xu, L. Yang, D. J. Cheng and D. P. Cao, *Small Methods*, 2019, **3**, 9.

14. I. S. Kwon, T. T. Debela, I. H. Kwak, Y. C. Park, J. Seo, J. Y. Shim, S. J. Yoo, J. G. Kim, J. Park and H. S. Kang, *Small*, 2020, **16**, 10.

15. X. Yang, Z. Zhao, X. Yu and L. Feng, *Chem. Commun.*, 2019, **55**, 1490-1493.

16. Z. Liu, X. Yang, G. Hu and L. Feng, *ACS Sustain. Chem. Eng.*, 2020, **8**, 9136-9144.

17. Y. Xu, X. Jiang, G. Shao, H. Xiang, S. Si, X. Li, T. S. Hu, G. Hong, S. Dong, H. Li, Y. Feng and S. Liu, *ENERGY & ENVIRONMENTAL MATERIALS*, 2021, **4**, 117-125.

18. U. Joshi, S. Malkhandi, Y. Ren, T. L. Tan, S. Y. Chiam and B. S. Yeo, *ACS Appl. Mater. Interfaces*, 2018, **10**, 6354-6360.

19. H. Liu, Z. Hu, Q. Liu, P. Sun, Y. Wang, S. Chou, Z. Hu and Z. Zhang, *J. Mater. Chem. A*, 2020, **8**, 24710-24717.

20. A. S. B. M. Najib, M. Iqbal, M. B. Zakaria, S. Shoji, Y. Cho, X. Peng, S. Ueda, A. Hashimoto, T. Fujita, M. Miyauchi, Y. Yamauchi and H. Abe, *J. Mater. Chem. A*, 2020, **8**, 19788-19792.

21. Y. Peng, B. Lu, L. Chen, N. Wang, J. E. Lu, Y. Ping and S. Chen, *J. Mater. Chem. A*, 2017, **5**, 18261-18269.

22. Z. Fan, J. Jiang, L. Ai, Z. Shao and S. Liu, *ACS Appl. Mater. Interfaces*, 2019, **11**, 47894-47903.